

RESEARCH ARTICLE

Evidence-Based Structural Model of the Staphylococcal Repressor Protein: Separation of Functions into Different Domains

Kinga Nyíri^{1,2*}, Bianka Kóhegyi^{1,2}, András Micsonai³, József Kardos³, Beata G. Vertessy^{1,2*}

1 Department of Applied Biotechnology and Food Sciences, Budapest University of Technology and Economics, Budapest, 1111, Hungary, **2** Institute of Enzymology, Research Centre for Natural Sciences, Hungarian Academy of Sciences, Budapest, 1117, Hungary, **3** Department of Biochemistry and MTA-ELTE NAP B Neuroimmunology Research Group, Institute of Biology, Eötvös Loránd University, Budapest, 1117, Hungary

* vertessy@mail.bme.hu; vertessy.beata@ttk.mta.hu (BGV); nyiri.kinga@ttk.mta.hu (KN)



CrossMark
click for updates

OPEN ACCESS

Citation: Nyíri K, Kóhegyi B, Micsonai A, Kardos J, Vertessy BG (2015) Evidence-Based Structural Model of the Staphylococcal Repressor Protein: Separation of Functions into Different Domains. *PLoS ONE* 10(9): e0139086. doi:10.1371/journal.pone.0139086

Editor: Eugene A. Permyakov, Russian Academy of Sciences, Institute for Biological Instrumentation, RUSSIAN FEDERATION

Received: June 25, 2015

Accepted: September 9, 2015

Published: September 28, 2015

Copyright: © 2015 Nyíri et al. This is an open access article distributed under the terms of the [Creative Commons Attribution License](http://creativecommons.org/licenses/by/4.0/), which permits unrestricted use, distribution, and reproduction in any medium, provided the original author and source are credited.

Data Availability Statement: All relevant data are within the paper and its Supporting Information files.

Funding: This study was supported by the Hungarian Scientific Research Fund OTKA [NK 84008, K109486]; Baross Program of the New Hungary Development Plan [3DSTRUCT, OMF-00266/2010 REG-KM-09-1-2009-0050]; Hungarian Academy of Sciences ([TTK IF-28/2012]; MedinProt program); CRP/HUN14-01 ICGEB Research Grant to BGV and the European Commission FP7 Biostruct-X project [contract No. 283570]. Funding for open

Abstract

Horizontal transfer of mobile genetic elements within *Staphylococci* is of high biomedical significance as such elements are frequently responsible for virulence and toxic effects. *Staphylococcus*-encoded repressor proteins regulate the replication of these mobile genetic elements that are located within the so-called pathogenicity islands. Here, we report structural and functional characterization of one such repressor protein, namely the StI protein encoded by the pathogenicity island SaPI_{bov1}. We create a 3D structural model and based on this prediction, we investigate the different functionalities of truncated and point mutant constructs. Results suggest that a helix-turn-helix motif governs the interaction of the StI protein with its cognate DNA site: point mutations within this motif drastically decrease DNA-binding ability, whereas the interaction with the StI-binding partner protein dUTPase is unperturbed by these point mutations. The 3D model also suggested the potential independent folding of a carboxy-terminal domain. This suggestion was fully verified by independent experiments revealing that the carboxy-terminal domain does not bind to DNA but is still capable of binding to and inhibiting dUTPase. A general model is proposed, which suggests that among the several structurally different repressor superfamilies StI-like Staphylococcal repressor proteins belong to the helix-turn-helix transcription factor group and the HTH motif is suggested to reside within N-terminal segment.

Introduction

Phage mediated mobilization of pathogenicity islands, i.e. genetic elements encoding virulence factors and toxins in *Staphylococcus aureus* (SaPI) has been an intensively studied field in recent years [1]. It has been shown that excision and replication of SaPIs is induced by formation of a repressor:derepressor complex constituting the Staphylococcal master repressor protein and another phage-related protein [2,3]. In the specific case of the SaPI_{bov1} pathogenicity

access charge: Hungarian Academy of Sciences. A. M. and J.K. were supported by the KTIA_NAP_13-2-2014-0017 program. SRCD experiments were supported by SOLEIL (Proposal No. 20140646).

Competing Interests: The authors have declared that no competing interests exist.

island repressor Stl (abbreviated as Stl in the present study), the derepressor is a phage-related dUTPase enzyme [3]. dUTPases are important guardians of genome integrity [4,5]. Their physiological role is to deplete the cellular dUTP pool to prevent incorporation of uracil into DNA [6,7]. The enzyme family of dUTPases constitutes two large subfamilies with different protein structure but very similar catalytic function [8,9].

In-depth studies on the Stl:dUTPase interaction revealed an additional function of the Stl repressor, namely it has been proven to be an effective inhibitor of the dUTPase enzyme from the Φ 11 Staphylococcal phage [10]. In addition, we have recently shown that Stl might be a cross-species general dUTPase inhibitor, which may open new horizons in studying dUTPase cellular function [11]. Moreover, since dUTPase has been proposed as a significant novel target in antimycobacterial drug design [12–14], Stl may also be a possible candidate for designing protein-based dUTPase-inhibitors to fight *Mycobacterium tuberculosis*.

For the dUTPase enzyme family, detailed studies have already addressed its structural and functional characteristics [8,15–21]. In contrast to the essential role of Stl-like repressors in the patho-mechanism and in the horizontal gene transfer of several toxins, no structural information has yet been reported for any of the SaPI repressor proteins or their complexes.

The SaPIs are generally considered as phage originated genetic elements, and this is supported by their mobilization by phage proteins. Similarly to master repressors of temperate phages Stl is an autoinducer [2], and blocks the expression of genes *int*, *xis* and *str*, which are responsible for SaPI excision and replication [22,23]. It has been shown that one of the DNA-binding sites of Stl resides within the *stl-str* intergenic region, which coincides with the repression of genes downstream to that region [22]. Other binding sites or sequence specificity of Stl have not been identified yet, however the question is intensively studied by our laboratory.

Based on functional similarities, the gene regulation mechanism of Stl may be adequately modeled by the mechanism of the main lifecycle regulator CI repressor of temperate phages. Within this model, repressor proteins are responsible for binding to a specific DNA segment thereby preventing excision and replication of the relevant genetic segments. The CI repressor proteins have separate domains for DNA binding and protein binding [24,25]. The protein binding domain is usually responsible for oligomerization of the repressor and for the interaction with the derepressor protein [24,26–28]. The oligomerization makes the regulation more sensitive to the alteration of protein concentration since it depends on the oligomer monomer equilibrium [28]. Higher order oligomers are suitable for more complex regulation patterns [29,30]. The mechanism of derepression can be reversible or irreversible. Prophage induction in lambdoid phages is achieved through a RecA binding induced specific autoproteolytic inactivation of the maintenance repressor [31]. Several P2 related repressors are inactivated through a noncovalent complex formation with the derepressor protein [32–35]. The DNA binding function of repressors can be performed through several different structural motifs, such as helix-turn-helix (HTH) as in CI repressor protein of lambda phage, winged-helix turn helix (wHTH) as in the MuR repressor protein of Mu phage, and the antiparallel β -strands of the ribbon-helix-helix (RHH) fold as in Arc repressor of P22 phage [36,37].

Based on these models, our focus was to resolve how potential domains within the Stl repressor may be defined. Towards this end, first we created a structural model of the full length Stl protein and investigated its folding by synchrotron radiation circular dichroism (SRCD) measurements. Based on the 3D model verified by CD results, we produced truncated and point mutants and studied their function in DNA and dUTPase binding. We show that the produced carboxy-terminal segment is an independently folded domain, which retains its binding affinity to dUTPase, but shows reduced inhibitory effect. The amino-terminal putatively DNA binding segment was also studied by point mutations. Our experimental results convincingly support the predicted position of helix-turn-helix motif.

Materials and Methods

Homology modeling and *in silico* predictions

The 3D homology model of Stl was constructed using the Phyre2 Server in intensive mode. Seven templates were selected by the program (PDB IDs: 1E3O, 4YV9, 2GRM, 4RYK, 2QFC, 2AXZ, 2EBY) to model Stl protein based on heuristics to maximize confidence, percentage identity and alignment coverage [38]. Five out of the seven templates covered >90% of the Stl sequence, while the other two templates provided only partial coverage of the sequence, but with higher local similarity. In the final model, 97% of residues were modeled at >90% confidence (see Table A in [S1 File](#) for additional information on the template proteins). Homology prediction was made using HHpred [39], subsequent 3D structure predictions with Modeller was performed with automatic template selection and also with the Phyre2 hits manually selected as templates from the HHpred list [40]. Related structures were searched in the Molecular Modeling Database (MMDB) also referred to as the Entrez Structure database [41]. Functional domain search was performed by Pfam and NCBI Conserved Domain Database [42,43]. The possible position of the helix-turn-helix (HTH) DNA binding motif in the sequence was predicted by NPS@ server [44]. Disorder prediction during construct design was performed by using GeneSilico MetaDisorder service [45]. To compare the homology model to the structural information obtained experimentally by SRCD spectroscopy, the secondary structure composition of the model, including the helix content, was assigned using the DSSP algorithm [46] and the BeStSel and CONTIN secondary structure definitions [47,48].

Cloning and expression of proteins

The cDNA of Stl-CTD was made by PCR amplification from the pGEX-4T-1 vector containing Stl protein (GenBank ID AAG29617.1) described in our previous work [10]. For the amplification of Stl-CTD the Stl-CTD-F (5'-TATTGAATTCAGCCCGACCCCTGAACG-3') and the Stl-CTD-R (5'-GGTCCTCGAGTT AGTTGGTATCTTTTTCCAGAATAATTTTTTCTGATG-3') primers were used. The resulting insert was cloned with EcoRI and XhoI restriction sites of the pGEX-4T-1 vector in frame with the amino-terminal GST tag and the thrombin cleavage site. A stop codon was mutated to the full length sequence to provide a construct for the N-terminal segment of Stl (residues 1–84) by QuikChange site-directed mutagenesis (Stratagene) using mutagenic primers Stl-NT-F 5'-GCGATGAATTTAAAGAAAAGGCTATTAGCTAACTGAGCCCGACCCCTGAACG-3') and Stl-NT-R 5'-CGTTCAGGGTCGGGCTCAGTTAGCTAATAGCCTTTTTCTTTAAATTCATCGC-3'. Stl-Q40A,N41A (Stl-AA) mutant was created from the original vector by QuikChange site-directed mutagenesis (Stratagene) using mutagenic primers Stl-AA-F 5'-CGTTTTTCATGGTTGCTAATGGTCGCTGCGCTAAAGCCGGTGCG-3') and Stl-AA-R 5'-CGCACCGGCTTTAGCGCAGCGACCATTAGCAACCATGAAAACG-3'. DNA sequencing for verification of the resulting constructs were performed by Eurofins MWG Operon. Vectors were transformed into *Escherichia coli* strain BL21 Rosetta (DE3) and propagated in 500 ml LB till exponential growth, then the culture was induced with 0.5 mM iso-propyl- β -D-thiogalactoside. After induction, the cell cultures were grown at 303 K for further 4 h. Finally the cells were harvested by centrifugation and stored at 193 K. Protein over-expression from the created constructs, except the one which encodes the N-terminal segment, was successful.

Purification of proteins

For purification of GST-tagged proteins (Stl, Stl-CTD, Stl-AA), cell pellets were solubilized using Potter-Elvehjem homogenizer in 20 ml buffer A (15 ml Hepes (pH 7.5), 200 mM NaCl)

supplemented with 2 mM dithiothreitol (DTT), 1% Triton X-100, ca. 2 µg/ml RNase and DNase and one tablet of Complete ULTRA Tablets, Mini, EDTA-free protease inhibitor. Cell suspensions were sonicated (4 x 60 s), and centrifuged (16000g for 30 min). Supernatant loaded on a pre-equilibrated benchtop glutathione-agarose affinity-chromatography column (GE Healthcare). The column was washed with ten volumes of buffer A (200 mM NaCl). After that 80 Cleavage Units thrombin (GE Healthcare) was added to perform on-column cleavage for the removal of GST tag. After overnight cleavage purified were obtained in the flow-through.

Purification of Φ 11dUTPase was performed as described previously [49]. Briefly, supernatant resulting from centrifugation of cell lysate was purified on Q-Sepharose (GE Healthcare) anion-exchange column, followed by gel filtration on a Superdex 75 column (GE Healthcare) using an AKTA Explorer purifier. Protein preparations were used freshly or were flash-frozen in liquid nitrogen, and stored at 193 K. All protein preparations were >95% pure as judged by SDS-PAGE.

Protein quantification

Protein concentration was measured using NanoDrop 2000 UV-Vis spectrophotometer using the following $A^{0.1\%}_{280}$ values 1.087, 1.261, 1.090 and 0.786 ml * mg⁻¹* cm⁻¹ for StI, StI-CTD, StI-AA and Φ 11dUTPase respectively, calculated based on amino acid composition (<http://web.expasy.org/protparam/>).

Native polyacrylamide gel electrophoresis

Native gel electrophoresis was performed in 8% polyacrylamide gel. After preparation the gel was subjected to pre-electrophoresis with constant voltages of 100 V. Then 25 µl of the pre-mixed samples was applied on the gel and electrophoresis was performed for 1.5 hours on 150 V in pH 8.7 Tris-HCl buffer. The apparatus was cooled on ice during electrophoresis in order to avoid denaturation caused by the evolving heat. Coomassie-Brilliant Blue dye washed to stain the gel.

Electrophoretic mobility shift assay (EMSA)

EMSA experiments were performed using a 57mer dsDNA oligonucleotide (5'-GCTCATAT TATTCCTCTCCTACCATTTTATCTCTAATTGAGATATTTATATTCAGAT-3') based on our previous results. Complementary oligonucleotides were custom synthesized by Eurofins MWG Operon and hybridized by controlled gradual cooling after 5 minutes incubation on 95°C. The investigated proteins were mixed with 100 ng DNA and in 20 µl total volume, concentration of NaCl was set to 100 mM in all the samples. After incubation for 15 min at 4°C, samples were loaded onto 8% polyacrylamide gel. Electrophoresis was performed in Tris-Borate- EDTA (TBE) buffer for 70 min at room temperature, following 1 h pre-electrophoresis of the gel. Bands were detected after staining with GelRed (Biotium), using a Uvi-Tec geldocumentation system (Cleaver Scientific Ltd., Rugby, UK).

Steady-state kinetics experiments

Proton release during the transformation of dUTP into dUMP and PPi was followed using a Jasco V550 spectrophotometer at 559 nm and 293 K [50]. Reaction mixtures contained 20 nM Φ 11 dUTPase enzyme in 1 mM HEPES-HCl (pH 7.5) containing 5 mM MgCl₂, 150 mM KCl and 40 mM phenol red pH indicator. After preincubation of the two proteins for 5 minutes the reaction was started with the addition of 20 mM dUTP. The initial velocity was determined

from the slope of the first 10% of the progress curve. Quadratic binding equation was fitted to the data.

Synchrotron radiation circular dichroism (SRCD) measurements and CD spectrum analysis

SRCD spectrum of StI was recorded at the DISCO beamline of SOLEIL French Synchrotron Facility (proposal No. 20140646). The StI concentration was 2.1 mg/ml in a buffer of 50 mM Hepes, 200 mM NaCl, pH 7.5. A CaF₂ cell with a path length of 6.13 μm was used. 38 scans were accumulated in the 180–270 nm wavelength range at 1 nm steps with a lock-in time constant of 300 msec and integration time of 1200 msec. In this wavelength range and path length, the photomultiplier voltage did not exceed the 700 V limit. After baseline subtraction, the spectrum was corrected with the CSA calibration [51].

To estimate the secondary structure content, the CD spectrum was analyzed by the BeStSel [47] and CONTIN methods [48]. These algorithms distinguish two types of spectrally different helical components, helix1 and helix2. Helix1 is the regular, middle part of the helix where all the backbone-backbone hydrogen bonds are formed and helix2, called “distorted helix”, consists of the two-two residues at the ends of the helix with unsatisfied H-bonding. The helix2 content together with the helix2/helix1 ratio provide a chance to predict the number and average length of helices in the protein [52]. We have to note that BeStSel defines helix as α-helix while the CONTIN definition includes α-helix and 3₁₀-helix. Usually the 3₁₀-helix content is low or absent and we expect similar results for the two algorithms.

Results and Discussion

StI protein is mainly α-helical

In lack of atomic resolution structural information, the structure of StI was analyzed by *in silico* methods and synchrotron radiation circular dichroism (SRCD) spectroscopy. The predicted homology model as provided by the Phyre2 Server [38] applying intensive mode is shown on Fig 1A, while the templates used for modeling are listed in Table A in S1 File. The StI sequence was entirely covered by alignment with the template sequences, with the exception of a very short part of the N-terminus (residues 1–7), which were modeled by *ab initio* methods. Apart

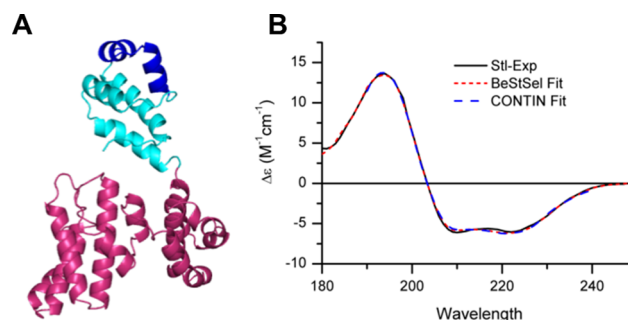


Fig 1. (A) Homology model of the StI protein. Ribbon representation of the homology model of the *Staphylococcus aureus* pathogenicity island repressor StI produced by Phyre2 Server [38]. Based on the homology model the protein is highly α helical (74%), and seems to be divided into two segments: the amino terminal segment colored cyan and the carboxy-terminal segment colored hotpink. According to Pfam and NCBI CDD the protein is predicted to contain a helix-turn-helix DNA binding motif. The position of the HTH predicted by NPS@ server is colored to dark blue [44]. **(B) SRCD spectrum of StI and fitted curves by BeStSel and CONTIN algorithms.** StI was measured at 2.1 mg/ml concentration in 50 mM Hepes, 200 mM NaCl, pH 7.5.

doi:10.1371/journal.pone.0139086.g001

from these first few residues the confidence of the alignment was more than 95%, so we assume that the overall fold and the core of the protein is modeled reliably, although the orientation of the surface loops are less well-defined. Based on this model, the repressor protein has a mostly α -helical (74%) secondary structure thus it is likely to belong to the class of “all- α ” proteins (SCOP ID 46456) that includes various protein superfamilies. Related structures found by the Molecular Modeling Database (MMDB) with E-value $> 10^{-6}$ (PDB ID: 2B5A, 3NTG, 2P5T) are also proteins with mostly α -helical fold [41]. Since the predicted fold type is shared by numerous proteins performing vast array of functions and the sequence identity between the templates and StI are relatively low, we did not analyze the template proteins in detail. To compare this model with others generated by alternative structural annotation servers StI sequence was submitted also to the HHpred predictor [39]. All templates used by Phyre2 (cf. Table A in S1 File) with the only exception of the human transcription factor Oct-1 were also within the list of closest homologs provided by HHpred. Following the HHpred search 3D structural models were generated by Modeller in two ways, i) with automatic template selection, which optimizes diversities of query and template HMMs, reranks templates and automatically selects best set, and ii) with the Phyre2 hits manually selected from the HHpred list as templates [40]. The first approach provided a well defined structural model only for the N-terminal residues (1–75), while the other resulted a structural model for almost all residues, however the C-terminal 33 residues are unstructured even in that model. Both the Phyre2 and the Modeller 3D structures agreed in that the protein is mostly α -helical and contains an N-terminal HTH motif (S1 Fig). However the orientation of the helices except the HTH was quite different in the two types of models.

Secondary structural elements of the full length StI protein were also experimentally characterized by CD spectroscopy. CD spectroscopy is a frequently used method to assess protein conformation: tertiary structural elements can be well reflected in the near-UV wavelength range (250–380 nm) [53], while secondary structural elements show well-known spectral characteristic in the far-UV wavelength range (180–240 nm) [48,54]. Due to the high far-UV absorption of the 200 mM NaCl in the buffer, these measurements were performed using synchrotron radiation CD (SRCD) providing extended wavelength range and increased signal/noise ratio compared to conventional CD measurements. The observed spectral shape was characteristic of α -helical proteins (Fig 1B). The secondary structure content was quantitatively estimated from the CD spectrum by the BeStSel [47] and CONTIN [48] algorithms showing

Table 1. Secondary structure estimation from the synchrotron radiation CD spectrum of StI and comparison to the homology model.

	BeStSel		CONTIN	
	CD analysis ^a	Model ^b	CD analysis ^a	Model ^b
Helix1	44.6	40.0	44.5	42.5
Helix2	23.0	21.4	18.8	21.4
β -sheet	3.6	0.0	6.3	0.0
Turn	8.4	7.5	9.0	10.4
Others	20.5	31.1	21.4	25.7
Number of helices	16	15	13	15
Average helix length	11.8	11.5	13.5	11.9

^aThe secondary structure composition from the CD spectrum was estimated by the BeStSel and CONTIN algorithms. The two algorithms use different secondary structure components, however, the overall helix, β -sheet and turn+others contents are comparable.

^bThe secondary structure contents were also calculated for the Phyre2 homology model using the DSSP algorithm [46] and the BeStSel and CONTIN definitions [47,48].

67.6 and 63.3% α -helix content respectively (Table 1). For both algorithms, the predicted β -sheet content was low, being close to zero within the accuracy of the methods. Only the Phyre2 model was suitable for a comparison to the results of the SRCD measurements since it provided a 3D model for the whole protein (Table 1). The StI Phyre-predicted 3D model shows similar secondary structural composition to that of the CD analysis within the experimental error supporting the reliability of the model. The two CD analysis methods also provided the possibility of estimation of the length and number of helical segments in the protein, which are in good agreement with the model, as well (Table 1). The accordance of the data obtained from the CD spectra and from the Phyre2 model, led us to consider this 3D model as a useful starting point for construct design and analysis tool for the StI-like proteins.

StI may possess two segments with distinct functions

The 3D homology model revealed that the StI protein— as numerous other repressors —seemingly consists of two segments, which may fold independently (Fig 1A). Pfam and NCBI CDD protein domain annotation engines [42,43] predicted that StI contains a helix-turn-helix DNA binding motif (HTH) at the amino-terminal part of the protein (between residues 15–68; with expectance value of $7.97 \cdot 10^{-11}$). The HTH was predicted to reside between residues 27–48 with 100% probability by NPS@ server [44]. In addition, we used the MetaDisorder server [45] to estimate flexibility characteristics of the StI protein (S2 Fig). Although these flexibility predictors provided rather different pattern, most agreed in indicating that a somewhat more ordered segment residues between residues 95–150, C-terminal to the HTH motif.

Based on these *in silico* predictions we hypothesized that the StI, similarly to other well-known repressors, possesses two segments, with putative distinct functions. We hypothesize that the amino-terminal segment encodes DNA binding function, while the carboxy-terminal segment may be responsible for other protein-protein interactions. In the context of the StI protein, complex formation with another protein partner, namely phage dUTPase was already shown to exist [10]. Hence, we speculated that this C-terminal segment may be involved in binding to phage dUTPase. We set out to investigate these suggestions and asked whether the N-terminal and C-terminal segments may fold independently and may still provide either DNA-binding or dUTPase-interacting function. To define the boundaries of the designed constructs, we relied on the i) the results from the flexibility annotation server (S2 Fig) ii) the Phyre2 structural prediction iii) length of the N-terminal protein constructs in experimentally determined three-dimensional structures of DNA-bound bacteriophage repressors [55–60]. With these considerations, a truncated construct encoding the C-terminal segment (residues 84–263) was produced by PCR based cloning and a stop codon was mutated to the full length sequence to obtain a construct for the N-terminal segment of StI (residues 1–84). The expression of N-terminal segment proved to be unsuccessful even if attaching this segment to a GST-tag, indicating that the N-terminus of StI, truncated at residue 85, may not fold independently. It was therefore not straightforward to analyze the N-terminal segment on its own. Hence we later took the approach to mutate the key residues in the HTH motif within the full-length context. The expression of the C-terminal segment was successful, indicating that this segment might be considered as an independently folded C-terminal domain (StI-CTD).

The StI-CTD domain is not capable of DNA-binding but binds and inhibits dUTPase

To check the suggested domain functions, the DNA binding ability of StI-CTD was investigated with electrophoretic mobility shift assay. Increasing concentrations (from 2 μ M up to 30 μ M) of StI-CTD was added to 100 ng DNA and mixtures were run on native PAGE gel (Fig 2A). No

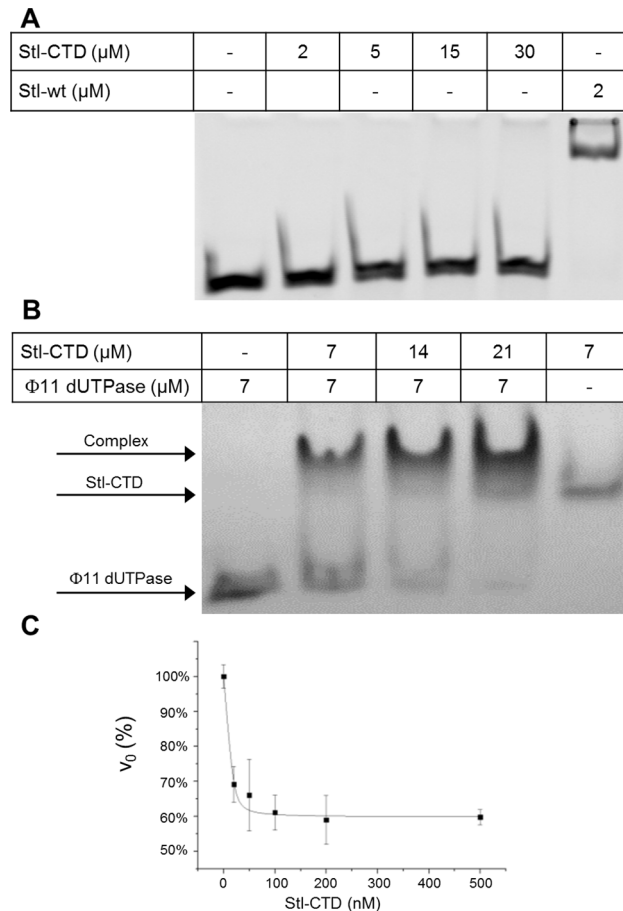


Fig 2. DNA and protein binding ability of StI-CTD. (A) Electrophoretic mobility shift assay was performed to investigate the DNA binding ability of StI-CTD. Species and concentrations given in monomers are indicated on the figure. The band of the dsDNA is only shifted upwards if wild type StI is added but there is no shift even at high concentrations StI-CTD. **(B) Native gel electrophoresis** experiment was performed to investigate the dUTPase binding ability of StI-CTD. Species and concentrations given in monomers are indicated. The mixture of StI-CTD and $\Phi 11$ dUTPase shows up in distinct position comparing to the individual proteins, which clearly indicate the complex formation. **(C) Activity of the $\Phi 11$ dUTPase** was measured in the presence and absence of StI-CTD. Each measurement was repeated three times. The quadratic binding equation was fit to the data resulted in the apparent $K_i = 1.5 \pm 0.5$ nM. The total change in amplitude of the activity was 40%.

doi:10.1371/journal.pone.0139086.g002

DNA shift was observed in any of the StI-CTD containing samples, while the positive control containing 2 μM StI clearly showed the expected shift due to complex formation between StI and DNA (cf Fig 3 in the present work and also Fig 2D in [10]).

The interaction of StI-CTD with $\Phi 11$ dUTPase was tested by two independent methods. Native polyacrylamide gel electrophoresis experiment was performed with the mixture of the two proteins (Fig 2B). Similarly to our previous results with wild type full length StI [10], the band corresponding to the complex of StI-CTD: $\Phi 11$ dUTPase shows up at a distinct position as compared to the positions of the two individual proteins. The interaction of the two proteins was also investigated by measuring the effect of StI-CTD on dUTPase activity (Fig 2C). StI-CTD inhibited the dUTPase activity with the apparent inhibitory constant of $K_i = 1.5 \pm 0.5$ nM. However, in contrast to wild type full length StI, which caused a practically complete loss of dUTPase activity if added in high excess [10], the maximum inhibitory effect exerted by StI-CTD on dUTPase was about 40% even at saturating inhibitor concentration. The difference in

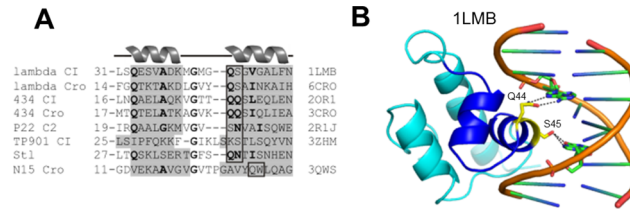


Fig 3. DNA binding domain of bacteriophage repressors. (A) Sequence alignment of the HTH motifs of bacteriophage repressors and StI. The number before each segment is the amino acid sequence number of the first residue in the sequence. Helices are with gray background, similar residues are in bold, box highlights residues interacting with DNA nucleobases. PDB ID of the proteins is indicated on the right side of the sequences. **(B) Experimentally determined structure of the DNA-bound CI bacteriophage repressor** DNA cartoons orange, protein cartoon: dark blue for HTHs, otherwise cyan. DNA bases and DNA interacting amino acid residues are stick representation with atomic coloring (protein carbon yellow, DNA carbon green, oxygen red, nitrogen blue, phosphorus orange.) The PDB ID of the structure is indicated. Stereo representation of all experimentally determined protein-DNA complex structures represented in the sequence alignment in this figure are available in [S3–S9 Figs](#).

doi:10.1371/journal.pone.0139086.g003

maximal dUTPase inhibition as compared to the wild type StI suggests that the amino-terminal segment of StI may also contribute to the interaction between the two proteins. In summary, these data show that the C-terminal segment of StI lacks the potential for DNA-binding while partially constitutes ability for dUTPase binding and inhibition. These observations suggest that while the C-terminal segment is capable folding on its own, it does not possess full functional capability for either of the two function of the full-length StI protein.

Specific point mutations within the putative helix-turn-helix motif of the StI N-terminal segment result in decreased DNA binding ability

To verify the prediction for a helix-turn-helix (HTH) motif, point mutations were performed within the StI protein to abolish DNA binding. Design of these mutations was based on experimentally determined three-dimensional structures of DNA-bound bacteriophage repressors. As of present, 3D structures for seven such proteins are available in the PDB, among these we have focused on the best resolution structures, for which the PDB IDs are as follow: 1LMB; 6CRO, 2OR1, 3CRO, 2RIJ, 3ZHM, 3QWS [55–60]. Besides the structural similarity of these phage repressor HTHs, five of those showed high level of sequence similarity to each other (Fig 3A), forming the basis of HTH prediction [44]. These structures together with numerous additional studies have established that the residues responsible for specific DNA binding are situated on the second helix of the HTH [61–63]. As shown on Fig 3A, with the exception of N15 phage Cro repressor, two residues could be identified as being conserved in different repressor-related HTH motifs, and moreover, in the published 3D structures, the role of these residues were also well defined. Namely, the first two residues of the second helix of the HTH motif provide H-bonding interaction with DNA nucleobases (Fig 3, S3–S9 Figs). In the StI protein, two similar polar residues show up at the same site within the predicted HTH motif (Fig 3A). In conclusion, based on the sequence alignment of the predicted StI HTH with different HTHs and the superimposition of the StI Phyre2 structural model on the crystal structures of these repressors, mutations of the polar residues Q40-N41 in the second helix were performed. To preserve the helical secondary structure while erasing the potential H-bonding ability, these two residues were exchanged into alanines. A similar double alanine mutational analysis was successfully performed with the TP901 repressor and yielded important insights [60].

According to the expectation, the double mutant (Q40-N41 – A40-A41) StI construct (termed as StI-AA) proved to be highly defective in DNA binding based on EMSA experiments

(Fig 4, S10 Fig). To verify that the double mutations within the HTH motif did not perturb dUTPase binding ability, we checked whether the double mutant protein may still form a complex with dUTPase. We showed that the complex between Stl-AA and dUTPase is readily observable on native polyacrylamide gel electrophoresis (S11 Fig). Also, dUTPase inhibition by the Stl-AA mutant has practically the same characteristics as compared to the inhibitory effect of wild type Stl (S12 Fig): the inhibitory constant has been determined to be 1.4 ± 0.9 nM, and the maximal inhibition was above 90%. Comparing to the wild type Stl the inhibition effect of Stl-AA on Φ 11 dUTPase is not perturbed [10]. Based on these findings, the design of an *in vivo* reporter system in progress in our laboratory to test Stl-DNA and Stl-dUTPase interactions.

General model for Stl-like repressors in *Staphylococci*

The group of Stl-like repressors has a major regulatory effect on the replication and subsequent horizontal transfer of mobile genetic elements in *Staphylococcal* strains. However, their structural and functional traits have not yet been addressed in details. In the present study, we have used the Phyre2 3D structural modeller software and the resulting model structure was in excellent agreement with experimentally determined structural elements via synchrotron radiation CD spectroscopy. Domain prediction based on this model did, in fact, make it possible to design an independently folding truncated construct (Stl-CTD). This domain lost DNA-binding capability but still preserved functionality with respect to binding and inhibition of dUTPase. Another *in silico* prediction method was also used with success in the present study: the

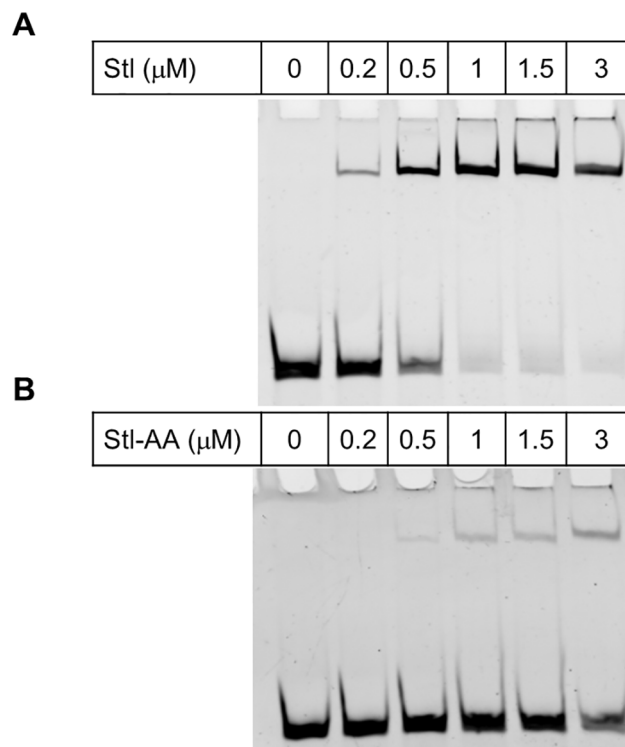


Fig 4. Electrophoretic mobility shift assay (EMSA) for testing the DNA binding ability of Stl constructs. (A) Result of EMSA with the wild type Stl protein. Note that the DNA band is shifted upwards at 1 μ M Stl concentration. **(B)** EMSA gel result of Stl-AA mutant protein. Note that even at relatively high (ie. 3 μ M) concentration of the Stl-AA mutant construct, most DNA still appears at the lower position on the gel, indicating lack of binding to the mutant protein.

doi:10.1371/journal.pone.0139086.g004

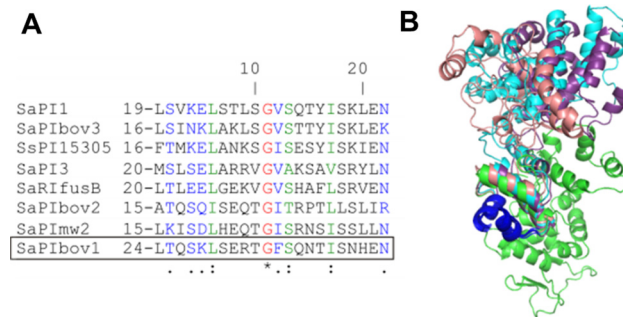


Fig 5. (A) Sequence alignment for the HTH segments of Stl-like repressors. Identical residues are in red (*), strongly similar (:) residues are in green, weakly similar residues are in blue (.). The protein investigated in the current study, termed as Stl throughout the text, is boxed (it is equivalent to the repressor of the SaPIbov1 pathogenicity island). **(B) Superimposed structural models of representative Stl-like repressors from different SaPIs.** Proteins are in cartoon representation. SaPIbov1 Stl is cyan, Stl-like repressors of SaPIbov3, SaPI1, and SsPI15305 pathogenicity islands are violetpurple, salmon, and green, respectively. Predicted HTH motifs of all proteins are colored dark blue. Stereo view of these structures is shown in [S14 Fig](#).

doi:10.1371/journal.pone.0139086.g005

HTH motif of Stl could be localized with confidence and this result could be fully ascertained by wetlab experiments (point mutations, EMSA and other assays).

Based on the success of these *in silico* predictions in the context of our Stl-focused study, we made an additional more generalized approach to decide if similar structural/functional elements may be identified in other representatives of the family of Stl-like repressors, as well. Towards this end, we first ran the HTH predictor on the different repressor protein sequences within the diverse *S. aureus* pathogenicity islands. [Fig 5](#) shows an alignment for the HTH motif identified in the diverse repressors: out of the 12 repressor sequences, HTH could be identified in 8 proteins with a probability above 50% (Table B in [S1 File](#)). In all of these cases, the HTH motif is located at the N-terminal part of the proteins.

It is worthwhile to point out that there is considerable sequence conservation within these HTH segments, while the other parts of these repressor proteins show high diversity (cf. [Fig 5](#) and [S13 Fig](#)). Protein Blast analysis of the Stl sequences did not find similarity among these proteins [64], however all of these were annotated as functioning as master repressors [65]. We have also used the Phyre2 modeler to build 3D models of these Stl-like repressors, to decide if these may possess similar 3D structures despite the high sequence diversity. Although these models are all characterized by a high α -helical content, i.e. similar folding pattern, the overall structures are still greatly diverse except for the well-conserved HTH motif (see structural models in [Fig 5](#)). It is rather probable that the HTH motifs are responsible for sequence-specific DNA binding in all of these repressors. For the case of the Sapibov1 Stl repressor, we have obtained detailed information of the mechanism of de-repression regulated by the dUTPase interacting partner [10]. Based on these data and the similar overall folding pattern, we propose that the carboxy-terminal domains of the other Stl-like repressors may constitute binding surface for interaction with other, yet unidentified proteins.

Supporting Information

S1 File. Document including Table A and Table B.
(DOCX)

S1 Fig. Comparison of the 3D models generated by Phyre2 and Modeller. (A) Ribbon representation of the homology model of the *Staphylococcus aureus* pathogenicity island repressor

StI produced by Phyre2 Server [38]. Based on the homology model the protein is highly α helical (74%), and seems to be divided into two segments: the amino terminal segment colored cyan and the carboxy-terminal segment colored hotpink. According to Pfam and NCBI CDD the protein is predicted to contain a helix-turn-helix DNA binding motif. The position of the HTH predicted by NPS@ server is colored to dark blue [44]. **(B)** Ribbon representation of the homology model of StI obtained by Modeller [40], predicted HTH colored yellow. **(C)** Superimposition of the two models. Both models agreed in that the protein is mostly α -helical and contains an N-terminal HTH motif.

(TIF)

S2 Fig. Disorder prediction and construct design. Representative curves from the results of flexibility prediction by MetaDisorder server are shown [45]. The mid-panel indicates our designed constructs represented as horizontal bars. Bottom-panel shows the secondary structure elements along the sequence, helices from the helix-turn-helix motif are in blue other helices are in purple.

(TIF)

S3 Fig. Experimentally determined structure of the DNA-bound lambda bacteriophage CI repressor (PDB ID 1LMB). DNA cartoons orange, protein cartoons: dark blue for HTHs, otherwise cyan. DNA bases and DNA interacting amino acid residues are stick representation with atomic coloring (protein carbon yellow, DNA carbon green, oxygen red, nitrogen blue, phosphorus orange.)

(TIF)

S4 Fig. Experimentally determined structure of the DNA-bound lambda bacteriophage Cro repressor (PDB ID 6CRO). Coloring as in S3 Fig.

(TIF)

S5 Fig. Experimentally determined structure of the DNA-bound 434 bacteriophage CI repressor (PDB ID 2OR1). Coloring as in S3 Fig.

(TIF)

S6 Fig. Experimentally determined structure of the DNA-bound 434 bacteriophage Cro repressor (PDB ID 3CRO). Coloring as in S3 Fig.

(TIF)

S7 Fig. Experimentally determined structure of the DNA-bound P22 bacteriophage C2 repressor (PDB ID 2R1J). Coloring as in S3 Fig.

(TIF)

S8 Fig. Experimentally determined structure of the DNA-bound TP901 bacteriophage CI repressor (PDB ID 3ZHM). Coloring as in S3 Fig.

(TIF)

S9 Fig. Experimentally determined structure of the DNA-bound N15 bacteriophage Cro repressor (PDB ID 3QWS) Coloring as in S3 Fig.

(TIF)

S10 Fig. Testing the DNA binding ability of StI-AA. Electrophoretic mobility shift assay was performed to investigate the DNA binding ability of StI-AA. Species and concentrations given in monomers are indicated on the figure. The band of the dsDNA is only partially sifted upwards even if high concentrations of StI-AA. Wild type StI shows shift of the same amount

of DNA at concentration of 1 μ M (cf. Fig 3).
(TIF)

S11 Fig. Testing the interaction of StI-AA with Φ 11 dUTPase on native-PAGE. Native gel electrophoresis experiment was performed to investigate the Φ 11 dUTPase binding ability of StI-AA. Species and concentrations given in monomers are indicated. Comparing to the wild type StI the complex formation of StI-AA with Φ 11 dUTPase is not perturbed (cf. Fig 1B. in [10]).
(TIF)

S12 Fig. Testing the inhibition of StI-AA with Φ 11 dUTPase. Enzyme activity Φ 11 dUTPase was measured in mixtures containing different concentrations of StI-AA. The inhibitory constant has been determined to be 1.4 ± 0.9 nM, and the maximal inhibition was above 90%. Comparing to the wild type StI the inhibition effect of StI-AA on Φ 11 dUTPase is not perturbed (cf. Fig 2A. in [10]).
(TIF)

S13 Fig. Alignment of different SaPI StI proteins. Identical residues are red (*). Strongly similar (:) residues are green, weakly similar residues are blue (.). Residues in the predicted HTH are underlined.
(TIF)

S14 Fig. Stereo view of superimposed structural models of representative StI-like repressors from different SaPIs. Proteins in cartoon representation. SaPIbov1 StI is cyan, StI-like repressors of SaPIbov3, SaPI1, and SsPI15305 pathogenicity islands are violetpurple, salmon, and green, respectively. Predicted HTH motifs of all proteins colored dark blue.
(TIF)

Acknowledgments

We thank Frank Wien and Matthieu Réfrégiers at DISCO beamline for their kind help in SRCD data collection.

Author Contributions

Conceived and designed the experiments: KN BGV. Performed the experiments: KN BK AM JK. Analyzed the data: KN BK AM JK BGV. Wrote the paper: KN AM JK BGV.

References

1. Lindsay JA, Ruzin A, Ross HF, Kurepina N, Novick RP. The gene for toxic shock toxin is carried by a family of mobile pathogenicity islands in *Staphylococcus aureus*. *Mol Microbiol.* 1998; 29: 527–543. doi: [10.1046/j.1365-2958.1998.00947.x](https://doi.org/10.1046/j.1365-2958.1998.00947.x) PMID: [9720870](https://pubmed.ncbi.nlm.nih.gov/9720870/)
2. Ubeda C, Maiques E, Barry P, Matthews A, Tormo MA, Lasa I, et al. SaPI mutations affecting replication and transfer and enabling autonomous replication in the absence of helper phage. *Mol Microbiol.* 2008; 67: 493–503. doi: [10.1111/j.1365-2958.2007.06027.x](https://doi.org/10.1111/j.1365-2958.2007.06027.x) PMID: [18086210](https://pubmed.ncbi.nlm.nih.gov/18086210/)
3. Tormo-Más MA, Mir I, Shrestha A, Tallent SM, Campoy S, Lasa I, et al. Moonlighting bacteriophage proteins derepress staphylococcal pathogenicity islands. *Nature.* 2010; 465: 779–82. doi: [10.1038/nature09065](https://doi.org/10.1038/nature09065) PMID: [20473284](https://pubmed.ncbi.nlm.nih.gov/20473284/)
4. Vértessy BG, Tóth J. Keeping Uracil Out of DNA: Physiological Role, Structure and Catalytic Mechanism of dUTPases. *Acc Chem Res.* 2009; 42: 97–106. doi: [10.1021/ar800114w.Keeping](https://doi.org/10.1021/ar800114w.Keeping) PMID: [18837522](https://pubmed.ncbi.nlm.nih.gov/18837522/)
5. Persson R, Cedergren-Zeppezauer ES, Wilson KS. Homotrimeric dUTPases; structural solutions for specific recognition and hydrolysis of dUTP. *Curr Protein Pept Sci.* 2001; 2: 287–300. doi: [10.2174/1389203013381035](https://doi.org/10.2174/1389203013381035) PMID: [12369926](https://pubmed.ncbi.nlm.nih.gov/12369926/)

6. Takács E, Grolmusz VK, Vértessy BG. A tradeoff between protein stability and conformational mobility in homotrimeric dUTPases. *FEBS Lett.* 2004; 566: 48–54. doi: [10.1016/j.febslet.2004.04.039](https://doi.org/10.1016/j.febslet.2004.04.039) PMID: [15147867](https://pubmed.ncbi.nlm.nih.gov/15147867/)
7. Muha V, Horváth A, Békési A, Pukáncsik M, Hodoscsek B, Merényi G, et al. Uracil-Containing DNA in *Drosophila*: Stability, Stage-Specific Accumulation, and Developmental Involvement. Hawley RS, editor. *PLoS Genet.* 2012; 8: e1002738. doi: [10.1371/journal.pgen.1002738](https://doi.org/10.1371/journal.pgen.1002738) PMID: [22685418](https://pubmed.ncbi.nlm.nih.gov/22685418/)
8. Vértessy BG, Zalud P, Nyman PO, Zeppezauer M. Identification of tyrosine as a functional residue in the active site of *Escherichia coli* dUTPase. *Biochim Biophys Acta.* 1994; 1205: 146–150. doi: [10.1016/0167-4838\(94\)90103-1](https://doi.org/10.1016/0167-4838(94)90103-1) PMID: [8142479](https://pubmed.ncbi.nlm.nih.gov/8142479/)
9. Hemsworth GR, González-Pacanowska D, Wilson KS. On the catalytic mechanism of dimeric dUTPases. *Biochem J.* 2013; 456: 81–8. doi: [10.1042/BJ20130796](https://doi.org/10.1042/BJ20130796) PMID: [24001052](https://pubmed.ncbi.nlm.nih.gov/24001052/)
10. Szabó JE, Németh V, Papp-Kádár V, Nyíri K, Leveles I, Bendes AA, et al. Highly potent dUTPase inhibition by a bacterial repressor protein reveals a novel mechanism for gene expression control. *Nucleic Acids Res.* 2014; 42: 11912–20. doi: [10.1093/nar/gku882](https://doi.org/10.1093/nar/gku882) PMID: [25274731](https://pubmed.ncbi.nlm.nih.gov/25274731/)
11. Hirmondó R, Szabó JE, Nyíri K, Tarjányi S, Dobrotka P, Tóth J, et al. Cross-species inhibition of dUTPase via the Staphylococcal Sfl protein perturbs dNTP pool and colony formation in *Mycobacterium*. *DNA Repair (Amst).* Elsevier B.V.; 2015; 30: 21–27. doi: [10.1016/j.dnarep.2015.03.005](https://doi.org/10.1016/j.dnarep.2015.03.005)
12. Varga B, Barabás O, Takács E, Nagy N, Nagy P, Vértessy BG. Active site of mycobacterial dUTPase: structural characteristics and a built-in sensor. *Biochem Biophys Res Commun.* 2008; 373: 8–13. doi: [10.1016/j.bbrc.2008.05.130](https://doi.org/10.1016/j.bbrc.2008.05.130) PMID: [18519027](https://pubmed.ncbi.nlm.nih.gov/18519027/)
13. Pecsí I, Hirmondó R, Brown AC, Lopata A, Parish T, Vértessy BG, et al. The dUTPase enzyme is essential in *Mycobacterium smegmatis*. *PLoS One.* 2012; 7: e37461. doi: [10.1371/journal.pone.0037461](https://doi.org/10.1371/journal.pone.0037461) PMID: [22655049](https://pubmed.ncbi.nlm.nih.gov/22655049/)
14. Horváti K, Bacsa B, Szabó N, Fodor K, Balka G, Rusvai M, et al. Antimycobacterial activity of peptide conjugate of pyridopyrimidine derivative against *Mycobacterium tuberculosis* in a series of in vitro and in vivo models. *Tuberculosis.* 2015; 95: 207–211. doi: [10.1016/j.tube.2015.02.026](https://doi.org/10.1016/j.tube.2015.02.026)
15. Cedergren-Zeppezauer ES, Larsson G, Nyman PO, Dauter Z, Wilson KS. Crystal structure of a dUTPase. *Nature.* Nature Publishing Group; 1992; 355: 740–3. doi: [10.1038/355740a0](https://doi.org/10.1038/355740a0) PMID: [1311056](https://pubmed.ncbi.nlm.nih.gov/1311056/)
16. Larsson G, Nyman PO, Kvassman JO. Kinetic characterization of dUTPase from *Escherichia coli*. *J Biol Chem.* 1996; 271: 24010–24016. doi: [10.1074/jbc.271.39.24010](https://doi.org/10.1074/jbc.271.39.24010) PMID: [8798636](https://pubmed.ncbi.nlm.nih.gov/8798636/)
17. Barabás O, Pongrácz V, Kovári J, Wilmanns M, Vértessy BG. Structural insights into the catalytic mechanism of phosphate ester hydrolysis by dUTPase. *J Biol Chem.* 2004; 279: 42907–15. doi: [10.1074/jbc.M406135200](https://doi.org/10.1074/jbc.M406135200) PMID: [15208312](https://pubmed.ncbi.nlm.nih.gov/15208312/)
18. Takács E, Barabás O, Petoukhov M V, Svergun DI, Vértessy BG. Molecular shape and prominent role of beta-strand swapping in organization of dUTPase oligomers. *FEBS Lett.* 2009; 583: 865–71. doi: [10.1016/j.febslet.2009.02.011](https://doi.org/10.1016/j.febslet.2009.02.011) PMID: [19302784](https://pubmed.ncbi.nlm.nih.gov/19302784/)
19. Pecsí I, Leveles I, Harmat V, Vértessy BG, Toth J. Aromatic stacking between nucleobase and enzyme promotes phosphate ester hydrolysis in dUTPase. 2010; 38: 7179–7186. doi: [10.1093/nar/gkq584](https://doi.org/10.1093/nar/gkq584) PMID: [20601405](https://pubmed.ncbi.nlm.nih.gov/20601405/)
20. Leveles I, Németh V, Szabó JE, Harmat V, Nyíri K, Bendes AA, et al. Structure and enzymatic mechanism of a moonlighting dUTPase. *Acta Crystallogr Sect D Biol Crystallogr.* International Union of Crystallography; 2013; 69: 2298–2308. doi: [10.1107/S0907444913021136](https://doi.org/10.1107/S0907444913021136)
21. Nagy GN, Leveles I, Vértessy BG. Preventive DNA repair by sanitizing the cellular (deoxy)nucleoside triphosphate pool. *FEBS J.* 2014; 281: 4207–23. doi: [10.1111/febs.12941](https://doi.org/10.1111/febs.12941) PMID: [25052017](https://pubmed.ncbi.nlm.nih.gov/25052017/)
22. Tormo-Más MÁ, Mir-Sanchis I, Shrestha A, Tallent SM, Campoy S, Lasa Í, et al. Moonlighting bacteriophage proteins derepress staphylococcal pathogenicity islands. *Nature.* 2010; 465: 779–82. doi: [10.1038/nature09065](https://doi.org/10.1038/nature09065) PMID: [20473284](https://pubmed.ncbi.nlm.nih.gov/20473284/)
23. Mir-Sanchis I, Martínez-Rubio R, Martí M, Chen J, Lasa Í, Novick RP, et al. Control of *Staphylococcus aureus* pathogenicity island excision. *Mol Microbiol.* 2012; 85: 833–45. doi: [10.1111/j.1365-2958.2012.08145.x](https://doi.org/10.1111/j.1365-2958.2012.08145.x) PMID: [22742067](https://pubmed.ncbi.nlm.nih.gov/22742067/)
24. Stayrook S, Jaru-Ampornpan P, Ni J, Hochschild A, Lewis M. Crystal structure of the lambda repressor and a model for pairwise cooperative operator binding. *Nature.* 2008; 452: 1022–5. doi: [10.1038/nature06831](https://doi.org/10.1038/nature06831) PMID: [18432246](https://pubmed.ncbi.nlm.nih.gov/18432246/)
25. Hochschild A, Lewis M. The bacteriophage lambda CI protein finds an asymmetric solution. *Current Opinion in Structural Biology.* 2009. pp. 79–86. doi: [10.1016/j.sbi.2008.12.008](https://doi.org/10.1016/j.sbi.2008.12.008) PMID: [19181516](https://pubmed.ncbi.nlm.nih.gov/19181516/)
26. Pinkett HW, Shearwin KE, Stayrook S, Dodd IB, Burr T, Hochschild A, et al. The structural basis of cooperative regulation at an alternate genetic switch. *Mol Cell.* 2006; 21: 605–15. doi: [10.1016/j.molcel.2006.01.019](https://doi.org/10.1016/j.molcel.2006.01.019) PMID: [16507359](https://pubmed.ncbi.nlm.nih.gov/16507359/)

27. Carlson PA, Koudelka GB. Expression, purification, and functional characterization of the carboxyl-terminal domain fragment of bacteriophage 434 repressor. *J Bacteriol.* 1994; 176: 6907–6914. PMID: [7961451](#)
28. Donner AL, Carlson PA, Koudelka GB. Dimerization specificity of P22 and 434 repressors is determined by multiple polypeptide segments. *J Bacteriol.* 1997; 179: 1253–1261. PMID: [9023209](#)
29. Révet B, Von Wilcken-Bergmann B, Bessert H, Barker A, Müller-Hill B. Four dimers of λ repressor bound to two suitably spaced pairs of λ operators form octamers and DNA loops over large distances. *Curr Biol.* 1999; 9: 151–154. doi: [10.1016/S0960-9822\(99\)80069-4](#) PMID: [10021390](#)
30. Bell CE, Lewis M. Crystal Structure of the λ Repressor C-terminal Domain Octamer. *J Mol Biol.* 2001; 314: 1127–1136. doi: [10.1006/jmbi.2001.5196](#) PMID: [11743728](#)
31. Roberts JW, Roberts CW. Proteolytic cleavage of bacteriophage lambda repressor in induction. *Proc Natl Acad Sci U S A.* 1975; 72: 147–151. doi: [10.1073/pnas.72.1.147](#) PMID: [1090931](#)
32. Shearwin KE, Brumby AM, Egan JB. The tum protein of coliphage 186 is an antirepressor. *J Biol Chem.* 1998; 273: 5708–5715. doi: [10.1074/jbc.273.10.5708](#) PMID: [9488703](#)
33. Heinzel T, Velleman M, Schuster H. C1 Repressor of phage P1 is inactivated by noncovalent binding of P1 coi protein. *J Biol Chem.* 1992; 267: 4183–4188. PMID: [1740459](#)
34. Heinzel T, Velleman M, Schuster H. The c1 repressor inactivator protein coi of bacteriophage P1: Cloning and expression of coi and its interference with c1 repressor function. *J Biol Chem.* 1990; 265: 17928–17934. PMID: [2211669](#)
35. Riedel HD, Heinrich J, Heisig A, Choli T, Schuster H. The antirepressor of phage P1. Isolation and interaction with the C1 repressor of P1 and P7. *FEBS Lett.* 1993; 334: 165–169. doi: [10.1016/0014-5793\(93\)81705-5](#) PMID: [8224242](#)
36. Rohs R, Jin X, West SM, Joshi R, Honig B, Mann RS. Origins of specificity in protein-DNA recognition. *Annu Rev Biochem.* 2010; 79: 233–269. doi: [10.1146/annurev-biochem-060408-091030](#) PMID: [20334529](#)
37. Wojciak JM, Iwahara J, Clubb RT. The Mu repressor-DNA complex contains an immobilized “wing” within the minor groove. *Nat Struct Biol.* 2001; 8: 84–90. doi: [10.1038/83103](#) PMID: [11135677](#)
38. Kelley L a, Sternberg MJE. Protein structure prediction on the Web: a case study using the Phyre server. *Nat Protoc.* 2009; 4: 363–71. doi: [10.1038/nprot.2009.2](#) PMID: [19247286](#)
39. Söding J. Protein homology detection by HMM-HMM comparison. *Bioinformatics.* 2005; 21: 951–60. doi: [10.1093/bioinformatics/bti125](#) PMID: [15531603](#)
40. Eswar N, Webb B, Marti-Renom MA, Madhusudhan MS, Eramian D, Shen M-Y, et al. Comparative protein structure modeling using Modeller. *Current Protocols in Bioinformatics.* John Wiley & Sons, Inc.; 2006. p. Unit 5.6. doi: [10.1002/0471250953.bi0506s15](#) PMID: [18428767](#)
41. Wang Y, Address KJ, Chen J, Geer LY, He J, He S, et al. MMDb: annotating protein sequences with Entrez’s 3D-structure database. *Nucleic Acids Res.* 2007; 35: D298–300. doi: [10.1093/nar/gkl952](#) PMID: [17135201](#)
42. Finn RD, Bateman A, Clements J, Coggill P, Eberhardt RY, Eddy SR, et al. Pfam: the protein families database. *Nucleic Acids Res.* 2014; 42: D222–30. doi: [10.1093/nar/gkt1223](#) PMID: [24288371](#)
43. Marchler-Bauer A, Derbyshire MK, Gonzales NR, Lu S, Chitsaz F, Geer LY, et al. CDD: NCBI’s conserved domain database. *Nucleic Acids Res.* 2014; 43: 222–226. doi: [10.1093/nar/gku1221](#)
44. Dodd IB, Egan JB. Improved detection of helix-turn-helix DNA-binding motifs in protein sequences. *Nucleic Acids Res.* 1990; 18: 5019–5026. doi: [10.1093/nar/18.17.5019](#) PMID: [2402433](#)
45. Kozlowski LP, Bujnicki JM. MetaDisorder: a meta-server for the prediction of intrinsic disorder in proteins. *BMC Bioinformatics.* BMC Bioinformatics; 2012; 13: 111. doi: [10.1186/1471-2105-13-111](#) PMID: [22624656](#)
46. Kabsch W, Sander C. Dictionary of protein secondary structure: pattern recognition of hydrogen-bonded and geometrical features. *Biopolymers.* 1983; 22: 2577–2637. doi: [10.1002/bip.360221211](#) PMID: [6667333](#)
47. Micsonai A, Wien F, Kernya L, Lee Y-H, Goto Y, Réfrégiers M, et al. Accurate secondary structure prediction and fold recognition for circular dichroism spectroscopy. *Proc Natl Acad Sci U S A.* 2015; 112: E3095–E3103. doi: [10.1073/pnas.1500851112](#) PMID: [26038575](#)
48. Provencher SW, Glöckner J. Estimation of globular protein secondary structure from circular dichroism. *Biochemistry.* 1981; 20: 33–37. doi: [10.1021/bi00504a006](#) PMID: [7470476](#)
49. Leveles I, Róna G, Zagyva I, Bendes Á, Harmat V, Vértessy BG. Crystallization and preliminary crystallographic analysis of dUTPase from the ϕ 11 helper phage of *Staphylococcus aureus*. *Acta Crystallogr Sect F.* 2011; 67: 1411–3. doi: [10.1107/S1744309111034580](#)

50. Vertessy BG. Flexible glycine rich motif of Escherichia coli deoxyuridine triphosphate nucleotidohydrolyase is important for functional but not for structural integrity of the enzyme. *Proteins Struct Funct Genet.* 1997; 28: 568–579. doi: [10.1002/\(SICI\)1097-0134\(199708\)28:4<568::AID-PROT10>3.0.CO;2-E](https://doi.org/10.1002/(SICI)1097-0134(199708)28:4<568::AID-PROT10>3.0.CO;2-E) PMID: [9261872](https://pubmed.ncbi.nlm.nih.gov/9261872/)
51. Chen GC, Yang JT. Two-Point Calibration of Circular Dichrometer with d-10-Camphorsulfonic Acid. *Anal Lett.* Taylor & Francis Group; 1977; 10: 1195–1207. doi: [10.1080/00032717708067855](https://doi.org/10.1080/00032717708067855) PMID: [21599305](https://pubmed.ncbi.nlm.nih.gov/21599305/)
52. Sreerama N, Venyaminov SY, Woody RW. Estimation of the number of alpha-helical and beta-strand segments in proteins using circular dichroism spectroscopy. *Protein Sci.* 1999; 8: 370–80. doi: [10.1110/ps.8.2.370](https://doi.org/10.1110/ps.8.2.370) PMID: [10048330](https://pubmed.ncbi.nlm.nih.gov/10048330/)
53. Orosz F, Kovács J, Löw P, Vértessy BG, Urbányi Z, Acs T, et al. Interaction of a new bis-indol derivative, KAR-2 with tubulin and its antimitotic activity. *Br J Pharmacol.* 1997; 121: 947–954. doi: [10.1038/sj.bjp.0701189](https://doi.org/10.1038/sj.bjp.0701189) PMID: [9222552](https://pubmed.ncbi.nlm.nih.gov/9222552/)
54. Whitmore L, Wallace BA. Protein secondary structure analyses from circular dichroism spectroscopy: methods and reference databases. *Biopolymers.* 2008; 89: 392–400. doi: [10.1002/bip.20853](https://doi.org/10.1002/bip.20853) PMID: [17896349](https://pubmed.ncbi.nlm.nih.gov/17896349/)
55. Beamer LJ, Pabo CO. Refined 1.8 Å crystal structure of the lambda repressor-operator complex. *J Mol Biol.* 1992; 227: 177–196. doi: [10.1016/0022-2836\(92\)90690-L](https://doi.org/10.1016/0022-2836(92)90690-L) PMID: [1387915](https://pubmed.ncbi.nlm.nih.gov/1387915/)
56. Albright RA, Matthews BW. Crystal structure of lambda-Cro bound to a consensus operator at 3.0 Å resolution. *J Mol Biol.* 1998; 280: 137–151. doi: [10.1006/jmbi.1998.1848](https://doi.org/10.1006/jmbi.1998.1848) PMID: [9653037](https://pubmed.ncbi.nlm.nih.gov/9653037/)
57. Aggarwal AK, Rodgers DW, Drottar M, Ptashne M, Harrison SC. Recognition of a DNA operator by the repressor of phage 434: a view at high resolution. *Science.* 1988; 242: 899–907. doi: [10.1126/science.3187531](https://doi.org/10.1126/science.3187531) PMID: [3187531](https://pubmed.ncbi.nlm.nih.gov/3187531/)
58. Shimon LJ, Harrison SC. The phage 434 OR2/R1-69 complex at 2.5 Å resolution. *J Mol Biol.* 1993; 232: 826–838. doi: [10.1016/0022-2836\(91\)90568-Q](https://doi.org/10.1016/0022-2836(91)90568-Q) PMID: [8355273](https://pubmed.ncbi.nlm.nih.gov/8355273/)
59. Watkins D, Hsiao C, Woods KK, Koudelka GB, Williams LD. P22 c2 repressor-operator complex: Mechanisms of direct and indirect readout. *Biochemistry.* 2008; 47: 2325–2338. doi: [10.1021/bi701826f](https://doi.org/10.1021/bi701826f) PMID: [18237194](https://pubmed.ncbi.nlm.nih.gov/18237194/)
60. Pedersen M, Lo Leggio L, Grossmann JG, Larsen S, Hammer K. Identification of quaternary structure and functional domains of the CI repressor from bacteriophage TP901-1. *J Mol Biol.* Elsevier Ltd; 2008; 376: 983–996. doi: [10.1016/j.jmb.2007.12.022](https://doi.org/10.1016/j.jmb.2007.12.022) PMID: [18191944](https://pubmed.ncbi.nlm.nih.gov/18191944/)
61. Isackson PJ, Bertrand KP. Dominant negative mutations in the Tn10 tet repressor: evidence for use of the conserved helix-turn-helix motif in DNA binding. *Proc Natl Acad Sci U S A.* 1985; 82: 6226–6230. doi: [10.1073/pnas.82.18.6226](https://doi.org/10.1073/pnas.82.18.6226) PMID: [2994067](https://pubmed.ncbi.nlm.nih.gov/2994067/)
62. Brennan RG, Matthews BW. The helix-turn-helix DNA binding motif. *J Biol Chem.* 1989; 264: 1903–1906. PMID: [2644244](https://pubmed.ncbi.nlm.nih.gov/2644244/)
63. Aravind L, Anantharaman V, Balaji S, Babu MM, Iyer LM. The many faces of the helix-turn-helix domain: transcription regulation and beyond. *FEMS Microbiol Rev.* 2005; 29: 231–62. doi: [10.1016/j.femsre.2004.12.008](https://doi.org/10.1016/j.femsre.2004.12.008) PMID: [15808743](https://pubmed.ncbi.nlm.nih.gov/15808743/)
64. Johnson M, Zaretskaya I, Raytselis Y, Merezhuik Y, McGinnis S, Madden TL. NCBI BLAST: a better web interface. *Nucleic Acids Res.* 2008; 36: W5–9. doi: [10.1093/nar/gkn201](https://doi.org/10.1093/nar/gkn201) PMID: [18440982](https://pubmed.ncbi.nlm.nih.gov/18440982/)
65. Novick RP, Christie GE, Penadés JR. The phage-related chromosomal islands of Gram-positive bacteria. *Nat Rev Microbiol.* 2010; 8: 541–51. doi: [10.1038/nrmicro2393](https://doi.org/10.1038/nrmicro2393) PMID: [20634809](https://pubmed.ncbi.nlm.nih.gov/20634809/)